Terahertz band-gap in InAs/GaSb type II superlattices

L.L. Li [1], W. Xu [1, 3], Z. Zeng [1], and Y.L. Shi [2]
[1] Key Laboratory of Materials Physics, Institute of Solid State Physics,
Chinese Academy of Sciences, Hefei 230031, China
[2] Kunming Institute of Physics, Kunming, China and
[3] Terahertz Research Center,
University of Electronic Science and Technology, Chengdu 610054, China

Abstract: We demonstrate theoretically that it is possible to realize terahertz (THz) fundamental band-gap between the electron mini-band in the InAs layer and the heavy-hole mini-band in the GaSb layer in InAs/GaSb based type II superlattices (SLs). The THz band-gap can be tuned by varying the sample growth parameters such as the well widths of the InAs and/or GaSb layers. The presence of such band-gap can result in a strong cut-off of optical absorption at THz frequencies. For typical sample structures, the THz cut-off of the optical absorption depends strongly on temperature and a sharper cut-off can be observed at relatively high-temperatures. This study is pertinent to the application of InAs/GaSb type II SLs as THz photodetectors. PACS numbers: 72.80.Cw, 72.20.Dp, 73.61.Cw

Keywords: THz band-gap, InAs/GaSb, type Ⅱ superlattices(SLs) , THz photodetectors

doi: 10.11906/TST.207-220.2008.12.17

1. Introduction

Terahertz (10^{12} Hz or THz) region is the most scientifically rich area of the electromagnetic (EM) spectrum[1]. The THz wave (or T-ray) technology is of great potential to impact many interdisciplinary fields such as telecommunication, biological science, pharmaceutical technology, anti-terrorist, nano-technology, to mention but a few. The realization of T-ray sources and sensors has been an important field of research in optics and optoelectronics since 1980's[2].

From a basic physics point of view, for the generation and detection of THz EM radiation, it is necessary to realize a material system in which the fundamental energy gap is around THz photon energy. Thus, THz generation and detection can be achieved through electronic transition accompanied by the emission and absorption of THz photons. In this paper, we propose to employ InAs/GaSb based type II superlattice (SL) systems as THz band-gap materials. In contrast to conventional semiconductor SL systems in which the conducting electrons and holes are located mainly in the same material layer, the confined electrons and holes in an InAs/GaSb type II SL are separated spatially in different well layers[3]. In such a SL structure, the energy-gap between the confined electron states in the InAs layer and the confined hole states in the GaSb layer can be tuned artificially by simply varying the sample growth parameters such as the widths of the InAs and GaSb layers. Thus, by band-gap engineering, we can realize a SL system in which the fundamental energy-gap between the valence (or hole) mini-band in the GaSb layer with the conduction (or electron) mini-band in the InAs layer at THz bandwidth. As a result, THz optical emission and absorption can be achieved via inter-layer transition among electron and hole states in different well layers (namely the type II transition). On the basis of such structures, THz optoelectronic devices can be designed and realized.

It should be noted that InAs/GaSb type II SLs have been proposed as uncooled midinfrared

(MIR) photodetectors working at 3-5 μm wavelength range for various applications[4]. It has been found experimentally that for short-period InAs/GaSb SLs with the well layer widths around 2.1/2.4 nm, sharp cut-off of the photoresponse can be observed at MIR bandwidth and the cut-off wavelength can be tuned by varying InAs/GaSb layer widths. In the present study, we generalize such SL systems for the application in the THz range. We believe this can shed light on the application of the InAs/GaSb type II SLs as advanced and practical THz devices such as THz photodetectors. The paper is organized as follows. In Section II, we present a simple model to calculate the electronic mini-band structure in InAs/GaSb type II SLs. The theoretical approach for the calculation of the optical absorption coefficient in a type II SL is developed in Section III. The results obtained from this investigation are presented and discussed in Section IV and the main conclusions drawn from this study are summarized in Section V.

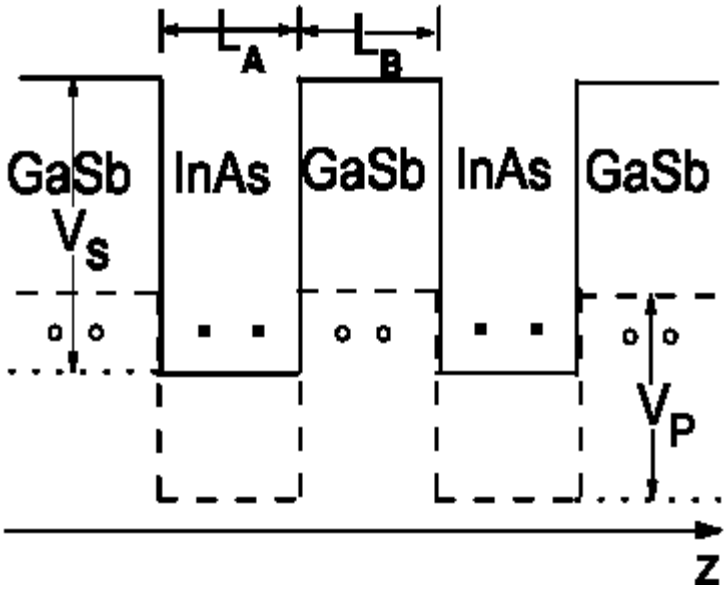

Fig. 1 Illustration of the band alignment for an InAs/GaSb type II SL along the growth direction (*z*-axis). Here, L_A and L_B are respectively the well widths for InAs and GaSb layers, and V_S and V_P are respectively the conduction and valence band offsets. The solid dots and open dots refer respectively to the bounded electrons and holes.

2. Electronic mini-band structure

In this study we generalize the standard Kronig-Penney model[5] to the calculation of the electronic mini-band structure of InAs/GaSb type II SLs. We consider an InAs/GaSb SL in which the growth direction is taken along the *z*-axis. The diagram of the band alignment along the growth direction for such an SL is illustrated in Fig. 1. In an InAs/GaSb type-II SL, the electrons and holes are separated spatially in the InAs and GaSb layers respectively. Here we employ the following notations to describe such an SL. L_A and L_B are respectively the InAs and GaSb layer thicknesses and, therefore, the periodicity of the SL is $d = L_A+L_B$. m_A and m_B are respectively effective masses for an electron or a hole in the InAs and GaSb layers. V_S (measured from the bottom of conduction band in InAs layer) and V_P (measured from the top of valence band in

GaSb layer) are respectively the conduction and valence band offsets which play the roles as the barriers for electrons and holes respectively. In the absence of scattering centers and external fields and neglecting the excitonic interactions between electrons and holes in the structure, the electron and hole mini-band structures can be solved separately. Firstly, we consider an electron confined within the InAs layers. Under the effective-mass approximation, the Schrödinger equation for an electron in the growth direction is

$$-\frac{\hbar^2}{2}\frac{d}{dz}\frac{1}{m(z)}\frac{d\psi(z)}{dz}+V(z)\psi(z)=\varepsilon\psi(z), \tag{1}$$

where the confining potential energy (see Fig. 1) is

$$V(z)=\begin{cases}0, & -L_A\le z\le 0;\\ V_s, & 0\le z\le L_B;\end{cases} \tag{2}$$

and

$$m(z)=\begin{cases}m_A, & -L_A\le z\le 0\\ m_B, & 0\le z\le L_B\end{cases} \tag{3}$$

is the electron effective-mass in different layers. The solution of Eq. (1) must obey the condition of the Bloch periodicity:

$$\psi(z+d)=e^{ik_z d}\psi(z), \tag{4}$$

with k_z= [$-\pi/d$, π/d] being the superlattice wavevector along the growth direction. In the zeroth period, the solution for a bound state $\varepsilon < V_S$ can be written as

$$\psi(z)=\begin{cases}c_1^A e^{ik_A z}+c_2^A e^{-ik_A z}, & -L_A\le z\le 0;\\ c_1^B e^{-ik_B z}+c_2^B e^{ik_B z}, & 0\le z\le L_B;\end{cases}, \tag{5}$$

Where $k_A=\sqrt{2m_A\varepsilon/\hbar^2}$ and $k_B=\sqrt{2m_B(V_S-\varepsilon)/\hbar^2}$.

Using the continuities of $\psi(z)$ and the weighted derivative $m^{-1}(z)d\psi(z)/dz$ at the InAs/GaSb interface and the condition of the Bloch periodicity, one obtains a 4×4 matrix

$$\begin{pmatrix}1 & 1 & -1 & -1\\ A & -A & -iB & iB\\ \mu^- & \mu^+ & -\nu^+ & -\nu^-\\ A\mu^- & -A\mu^+ & -iB\nu^+ & iB\nu^-\end{pmatrix}\begin{pmatrix}c_1^A\\ c_2^A\\ c_1^B\\ c_2^B\end{pmatrix}=0, \tag{6}$$

where $A = k_A/m_A, B = k_B/m_B, \mu^{\pm} = e^{i(k_z d \pm k_A L_A)}$ *and* $\nu^{\pm} = e^{\mp k_B L_B}$. For a nontrivial solution of Eq. (6), the 4 × 4 determinant of the corresponding matrix must be zero, which results in the Kronig-Penney equation for an electron in a bound state $\varepsilon < V_S$

$$\begin{aligned}\cos(k_z d) = \frac{1}{2}\left(\beta - 1/\beta\right)\sin(k_A L_A)\sinh(k_B L_B) \\ + \cos(k_A L_A)\cosh(k_B L_B),\end{aligned} \tag{7}$$

where $\beta = B/A$. The corresponding electron wavefunction can be rewritten as

$$\psi(z) = \begin{cases} \cos(k_A z) + \beta F \sin(k_A z), & -L_A \le z \le 0; \\ \cosh(k_B z) + F \sinh(k_B z), & 0 \le z \le L_B, \end{cases} \tag{8}$$

where

$$F = \frac{\cos(k_A L_A)e^{ik_z d} - \cosh(k_B L_B)}{\beta \sin(k_A L_A)e^{ik_z d} + \sinh(k_B L_B)}$$

and A is determined by normalization condition: $\int_{-L_A}^{L_B} \psi^*(z)\psi(z)dz = 1$.

Using the Kronig-Penney equation given by Eq. (7), the energy for an electron in the n^{th} mini-band in the InAs layer, $\varepsilon^e = \varepsilon_n^e(k_z)$, can be determined and, then, from it the corresponding wavefunction, $\psi^e = \psi_{nk_z}^e(z)$ can be obtained. Using the similar approach the energy, $\varepsilon_n^h(k_z)$ and wavefunction, $\psi_{nk_z}^h(z)$, for a hole in the n^{th} mini-band in the GaSb layer can also be calculated.

3. Optical absorption coefficient

In an SL, the wavefunction and energy spectrum for an electron ($j = e = 2$) or a hole ($j = h = 1$) can be written, respectively, as

$$\begin{cases} \Psi_{nK}^j(\mathbf{R}) = e^{i\mathbf{k}\cdot\mathbf{r}}\psi_{nk_z}^j(z), \\ E_n^j(\mathbf{K}) = (-1)^j \hbar^2 k^2 / 2m_j^* + \varepsilon_n^j(k_z), \end{cases} \tag{9}$$

where $\mathbf{R} = (\mathbf{r}, z) = (x, y, z)$, $\mathbf{K} = (\mathbf{k}, k_z) = (k_x, k_y, k_z)$ with $\mathbf{k}$ being the electron/hole wavevector along the xy-plane and k_z the wavevector of the reciprocal space along the growth direction, and m_j^* is the density-of-states effective-mass for an electron or a hole. We now consider that an EM field, which is polarized linearly along the z-direction, is applied to the SL. Applying the electron and hole wavefunctions and energy spectra given by Eq.(9) into the Fermi's golden rule, the

electronic transition rate induced by direct interactions between electrons/holes and the radiation field via absorption scattering is obtained as $W_{nn'}^{jj'}(K,K') = W_{nn'}^{jj'}(K)\delta_{K',K}$, where

$$W_{nn'}^{jj'} = \frac{2\pi}{\hbar}\left(\frac{e\hbar F_0}{m_j^* \omega}\right)^2 \left|X_{nn'}^{jj'}(k_z)\right|^2 \delta\left[E_n^j(\mathbf{K}) - E_{n'}^{j'}(\mathbf{K}) + \hbar\omega\right], \tag{10}$$

which measures the probability for scattering of an electron or a hole at a state $|n,\mathbf{K}\rangle$ in layer j to a state $|n',\mathbf{K}'\rangle$ in layer j'. Here, F_0 and ω are, respectively, the electric field strength and frequency of the EM field, and $X_{nn'}^{jj'}(k_z) = \int dz \psi_{n'k_z}^{j'*}(z)\left[d\psi_{n'k_z}^{j}(z)/dz\right]$ is the form factor for electron/hole coupling with a photon. The term $\delta_{K',K}$ reflects the fact that the direct electron/hole-photon coupling in an SL does not change the momentum of an electron or a hole.

In this paper, we employ the semi-classic Boltzmann equation as the governing transport equation to study the response of the carriers (electrons and holes) in an SL to the applied radiation field. For an electron or a hole, the Boltzmann equation in a degenerate statistics take a form

$$\frac{\partial f_n^j(\mathbf{K},t)}{\partial t} = g_s \sum_{j',\mathbf{K}',n'}\left[F_{n'n}^{j'j}(\mathbf{K}',\mathbf{K},t) - F_{nn'}^{jj'}(\mathbf{K},\mathbf{K}',t)\right]. \tag{11}$$

Here, g_s = 2 counts for spin-degeneracy, $F_{n'n}^{j'j}(\mathbf{K}',\mathbf{K},t) = f_n^j(\mathbf{K},t)\left[1 - f_{n'}^{j'}(\mathbf{K},t)\right]W_{nn'}^{jj'}(\mathbf{K},\mathbf{K}')$, $f_n^j(\mathbf{K},t)$, is the momentum-distribution functions for a carrier at a state $|\mathbf{K},n\rangle$ in layer j, and $W_{nn'}^{jj'}(\mathbf{K},\mathbf{K}')$ is the steady-state electronic transition rate. In Eq. (11), the effect of the EM field has been included within the time-dependent electron/hole distribution functions and within the electronic transition rate. Thus, to avoid double counting, the force term induced by the EM field does not appear on the left-hand side of the Boltzmann equation. It is known that there is no simple and analytical solution to Eq. (11) with the electronic transition rate given by Eq. (10). In this work, we apply the usual balance-equation approach to solve the problem[6]. For the first moment, the energy-balance equation[7] can be derived by multiplying $g_S \sum_n \sum_K E_n^j(\mathbf{K})$ to both sides of Eq. (11). In doing so, we obtain two energy-balance equations respectively for an electron and a hole and, from them, the total electronic energy transfer rate due to electron/hole interactions with photons is obtained as

$$P = p_e + p_h = \sum_{j,j'} P_{jj'}, \tag{12}$$

where $p_j = g_S \partial\left[\sum_n \sum_{\mathbf{K}} E_n^j(\mathbf{K}) f_n^j(\mathbf{K},t)\right]/\partial t$ is the electronic energy transfer rate per cell of the SL for electrons or holes and

$$P_{jj'} = 4\hbar\omega \sum_{n',n,\mathbf{K}} f_j(E_n^j(\mathbf{K}))\left[1 - f_{j'}(E_{n'}^{j'}(\mathbf{K}))\right] W_{nn'}^{jj'}(\mathbf{K}). \tag{13}$$

Here we have used a statistical energy distribution such as the Fermi-Dirac function as electron/hole distribution function at a steady-state. Namely, we have taken $f_n^j(K,t) \approx f_j\left(E_n^j(K)\right)$ where $f_j(x) = \left[e^{\left(x-\mu_j^*\right)/k_BT} + 1\right]^{-1}$ is the Fermi-Dirac function with μ_j^* being the Fermi energy (or chemical potential) for an electron or a hole. The optical absorption coe.cient induced by electron and hole interactions with the EM field can be calculated through[8]

$$\alpha = \alpha_0\left(2\hbar P / e^2\sqrt{\kappa_j}F_0^2\right) = \sum_{j,j'}\alpha_{jj'}, \tag{14}$$

where $\alpha = e^2/(\hbar\varepsilon_0 C)$, k_j and ε_0 are respectively the dielectric constants of the material j and the free space, and C is the velocity of the light in vacuum. Thus, the optical absorption coefficients induced by intra- (i.e., $j = j'$) and inter-layer (i.e., $j \neq j'$) transition are obtained respectively as

$$\begin{aligned}\alpha_{jj} = \alpha_0 c_j \sum_{n',n,K} & f_j(E_n^j(\mathbf{K}))\left[1 - f_{j'}(E_{n'}^{j'}(\mathbf{K}))\right]\left|X_{nn'}^{jj'}(k_z)\right|^2 \\ & \times\delta\left[\varepsilon_n^j(k_z) - \varepsilon_{n'}^j(k_z) + \hbar\omega\right],\end{aligned} \tag{15}$$

and

$$\begin{aligned}\alpha_{jj'} = \alpha_0\gamma_j(M^*/m_j^*)\sum_{n',n,\mathbf{K}} & \Theta\left[\varepsilon_n^j(k_z) - \varepsilon_{n'}^j(k_z) + \hbar\omega\right] \\ & \times f_j(x_{j'}^-)\left[1 - f_{j'}(x_j^+)\right]\left|X_{nn'}^{jj'}(k_z)\right|^2,\end{aligned} \tag{16}$$

where $c_j = 16\pi\hbar^3/\omega\sqrt{\kappa_j}\,(m_j^*)^2$, $1/M^* = 1/m_e^* + 1/m_h^*$, $\gamma_j = 8\hbar/(m_j^*\sqrt{k_j}\,\omega)$ and $x^{\pm} = \left[m_e^*\varepsilon_n^e(k_z) + m_h^*\varepsilon_{n'}^h(k_z) \pm m_j^*\hbar\omega\right]/(m_e^* + m_h^*)$. As can be seen from Eqs. (15) and (16), if we know the wavefunctions and energy spectra for an electron and a hole in an SL analytically the optical absorption coefficient can be calculated easily with the simple approach developed here.

4. Numerical results and discussions

4.1. THz miniband structure

In this work, we generalize the usual Kronig-Penney model[5] (see Section II) to calculate the electronic mini-band structure of InAs/GaSb based type II SLs. From this calculation, we can obtain the wavefunction $\psi_{nk_z}^j(z)$ and energy $\varepsilon_n^j(k_z)$ for an electron ($j = e$) or a heavy-hole ($j =$

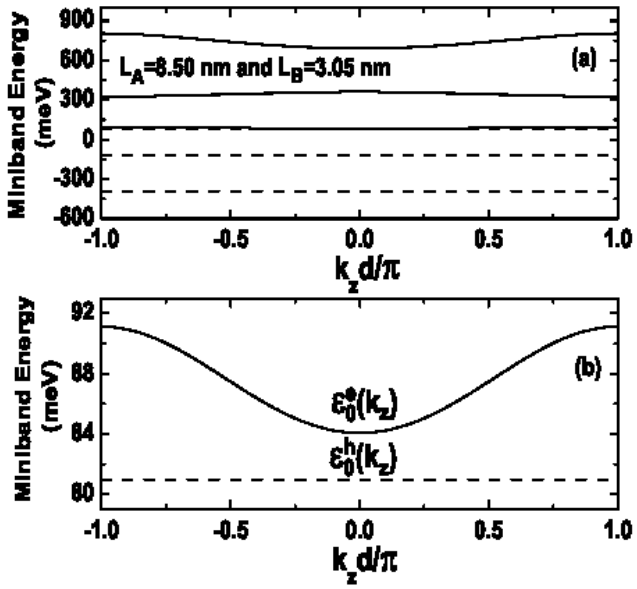

Fig. 2 (a) Dispersion relations of the electron/hole mini-band energies, $\varepsilon_n^e(k_z)/\varepsilon_n^h(k_z)$ (solid/dashed curves), for the fixed InAs/GaSb layer widths L_A/L_B as indicated. (b) Corresponding dispersion relations for the lowest electron mini-band in the InAs layer, $\varepsilon_0^e(k_z)$, and the highest heavy-hole mini-band in the GaSb layer, $\varepsilon_0^h(k_z)$.

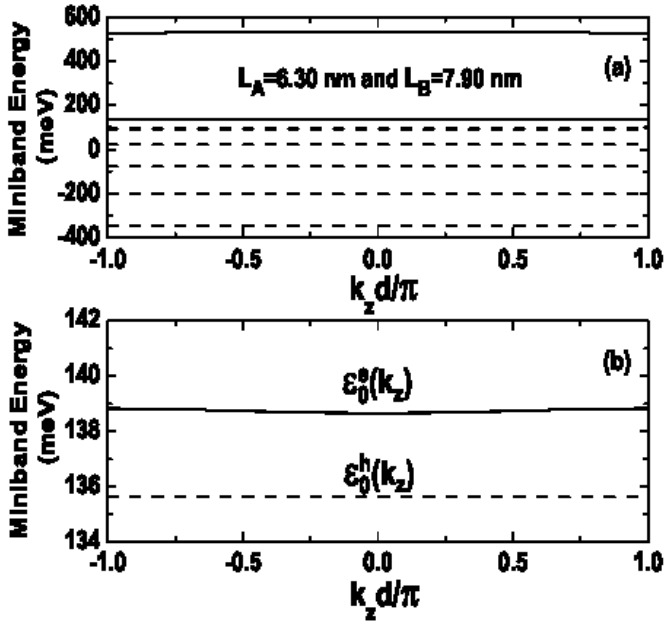

Fig.3 The same as in Fig. 2 but with different InAs/GaSb layer widths L_A/L_B as indicated.

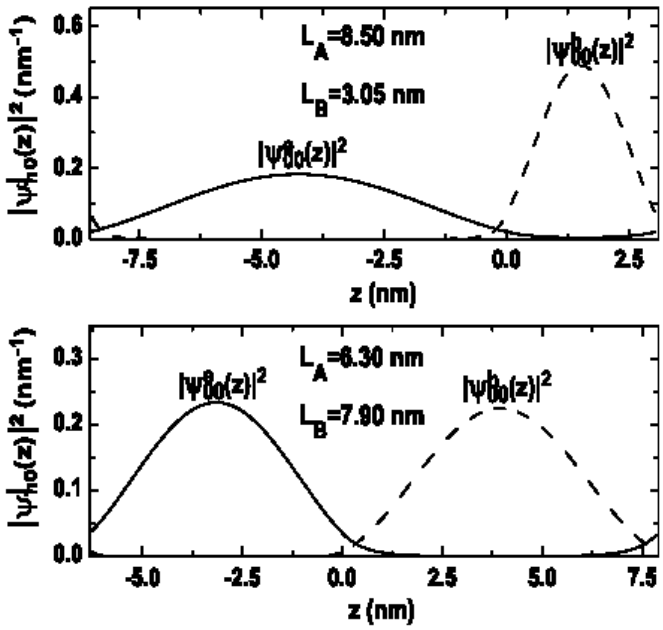

Fig.4 Square module of the electron/hole wavefunctions at $k_z = 0$, $\psi^e_{n0}(z)/\psi^h_{n0}(z)$ (solid/dashed curves), as a function of the distance *z* for the fixed InAs/GaSb layer widths L_A/L_B as indicated. Here z = 0 is at the interface between the InAs and GaSb layers.

h) in the n^{th} miniband in the SL, with k_z being the SL wavevector along the growth direction (or the z-axis). The effective masses for carriers (electrons and holes) in InAs/GaSb SLs are taken as: $m^*_e(InAs) = m^e_A = 0.038m_0$ with m_0 being the rest electron mass, $m^*_h(InAs) = m^h_A = 0.40m_0$, $m^*_e(GaSb) = m^e_B = 0.040m_0$ and $m^*_h(GaSb) = m^h_B = 0.33m_0$. In the calculation, we take the conduction-and-valence-band offsets at the InAs/GaSb interfaces to be $V_S = \Delta E_C = 960meV$ and $V_P = \Delta E_V = 450meV$ and the conduction-and-valence-band overlap energy is $\Delta = 150meV$. These band parameters have led to a good agreement between the experimental and theoretical results in InAs/GaSb based type II quantum well systems[9,10]. In Fig. 2, we show the dependence of the mini-band energies in an InAs/GaSb SL on k_z the wavevector of the reciprocal space along the growth direction. We find that when the InAs/GaSb layer widths are around L_A/L_B = 8.50/3.05 nm, there are three mini-bands $\varepsilon^e_n(k_z)$ (n=0, 1 and 2) for electrons in the InAs layer and there are the same number of the mini-bands $\varepsilon^h_n(k_z)$ (n=0, 1 and 2) for heavy-holes in the GaSb layer. $\varepsilon^e_n(k_z)$ depends rather strongly on k_z whereas $\varepsilon^h_n(k_z)$ depends little on k_z, due to the fact that a heavy-hole has a larger effective mass than an electron has and the GaSb layer is relatively narrow. From Fig. 2(b), we see that the energy-gap between the bottom of the lowest electron mini-band in the InAs layer and the top of the highest heavy-hole mini-band in the GaSb layer is about 3 meV, which is located in the THz bandwidth. The dispersion relations for the electron/hole mini-band energies with another InAs/GaSb SL growth parameters, L_A/L_B = 6.30/7.90 nm, are shown in Fig. 3. We see that with such growth parameters, the THz band-gap can also be realized between the bottom of the lowest electron mini-band in the InAs layer and the top of the highest heavy-hole mini-band in the GaSb layer. However, when L_A/L_B = 6.30/7.90

nm, there are two mini-bands for electrons in the InAs layer and six mini-bands for heavy-holes in the GaSb layer.

For the applications of the type II SLs as electronic and optical devices, it is necessary to know the strength of the overlap of the electron and hole wavefunctions at the interfaces between InAs and GaSb well layers. In Fig. 4, we show the electron and hole wavefunctions at $k_z = 0$ for two InAs/GaSb SLs with layer widths L_A/L_B = 8.50/3.05 nm and 6.30/7.90 nm respectively. As can be seen, in an InAs/GaSb type II SL, the electrons and holes are confined predominantly in the InAs- and GaSb- layers respectively. The hole distribution is more localized than the electron distribution, as a result of the quantum size effect and different effective masses. Comparing the upper and lower panels in Fig. 4, we find that the electronic tunneling effect in the upper case is stronger than that in the lower case, due to the narrower GaSb layer width in the upper case. This results in a fact that the electron mini-band energies are more dispersed in Fig. 2 than those in Fig. 3. It should be noted that for samples with THz band-gap energies, owing to their relatively larger well widths L_A/L_B, the overlaps of the electron and hole wavefunctions at the InAs/GaSb interfaces are significantly less than those in samples with MIR band-gap where L_A/L_B ~ 2.1/2.4 *nm*.

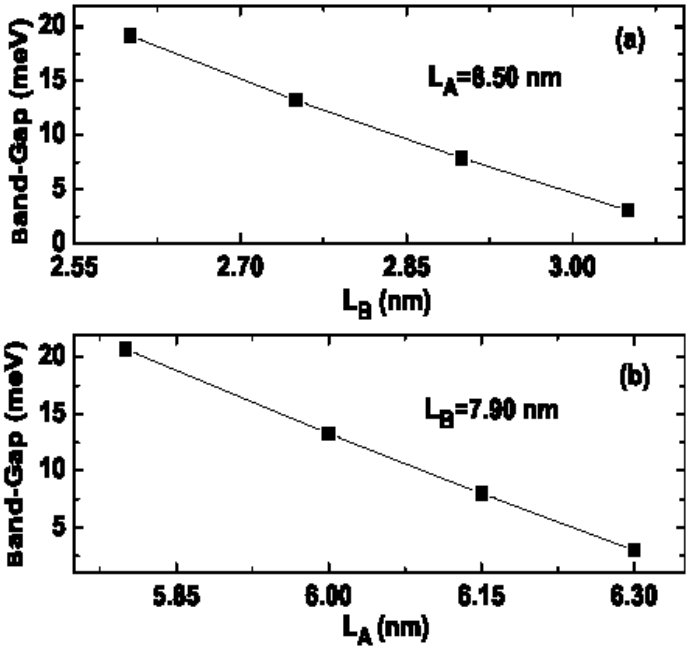

Fig.5 Band-gap energy between the bottom of the lowest electron mini-band in the InAs layer and the top of the highest heavy-hole mini-band in the GaSb layer as a function of GaSb (InAs) layer width L_B (L_A) at a fixed InAs (GaSb) layer width, in the upper (lower) panel. The results are shown for $k_z = 0$.

In Fig. 5, we show the band-gap energy between the bottom of the lowest electron miniband in the InAs layer and the top of the highest heavy-hole mini-band in the GaSb layer as a function of the InAs (GaSb) layer width at a fixed GaSb (InAs) well thickness. It is found that there are two sets of growth parameters which can be used to reach THz band-gap in InAs/GaSb type II SLs. When the InAs/GaSb layer widths are about 8.50/2.80 nm or 6.10/7.90 nm, the fundamental

band-gap $E_g = \varepsilon_0^e(0) - \varepsilon_0^h(0)$ is of the order of THz and can be tuned by adjusting the InAs/GaSb layer widths. The band-gap energy E_g decreases with increasing the InAs and/or GaSb layer thickness, because the energy of the electron miniband in the InAs layer decreases with increasing L_A and that of the heavy-hole mini-band in the GaSb layer increases with L_B. Furthermore, we find that in these sample structures, the energy separations among the electron and hole mini-bands in different layers [i.e., $\varepsilon_m^j(k_z) - \varepsilon_n^j(k_z)$] are larger than 100 *meV*, namely they are in the mid-infrared bandwidth. This suggests that intra-layer electronic transition does not affect significantly the THz range.

4.2. Optical absorption spectrum

In a undoped InAs/GaSb type II SL, the presence of the radiation field can pump electrons in the valance band in the GaSb layer into the conduction band in the InAs layer. Such process induces photo-excited carriers whose transitions contribute mainly to the optical absorption in the SL. In general, the density of photo-excited carriers depends on the radiation intensity and frequency and on other scattering and relaxation mechanisms. In this study, we assume that the photo-excited carrier density in undoped SLs is about $n_e = n_h \sim 2\times10^{17} cm^{-3}$ per SL cell, which satisfies the condition of the charge-neutrality. Because in an InAs/GaSb SL the electron and heavy-hole have different effective masses, the non-equilibrium chemical potentials (i.e., μ_j^* induced by the presence of photo-excited carriers) for electrons and holes are different. Introducing the energy spectrum for an electron or a hole in a SL into the corresponding density-of-states, the non-equilibrium chemical potential μ_e^* / μ_h^* in the presence of the radiation field can be calculated, respectively, through

$$n_e = g_s \sum_{n,\mathbf{K}} f_e(E_n^e(\mathbf{K})) = \lambda_e \sum_{n,k_z} \ln\left\{1 + \exp\left[\frac{\mu_e^* - \varepsilon_n^e(k_z)}{k_B T}\right]\right\}, \tag{17}$$

and

$$n_h = g_s \sum_{n,\mathbf{K}} (1 - f_h(E_n^h(\mathbf{K}))) = \lambda_h \sum_{n,k_z} \ln\left\{1 + \exp\left[\frac{\varepsilon_n^h(k_z) - \mu_h^*}{k_B T}\right]\right\}, \tag{18}$$

where n_j is the carrier density and $\lambda_j = m_j^* k_B T / \pi\hbar^2$. In Fig. 6, we show the temperature dependence of the chemical potentials for electrons (μ_e^*)in the InAs layer and heavy-holes (μ_h^*) in the GaSb layer in an InAs/GaSb type II SL at a fixed carrier density $n_e = n_h = 2\times10^{17} cm^{-3}$. As can be seen, $\mu_e^*(\mu_h^*)$ decreases (increases) with increasing temperature. This feature is in line with those observed in the conventional SL systems.

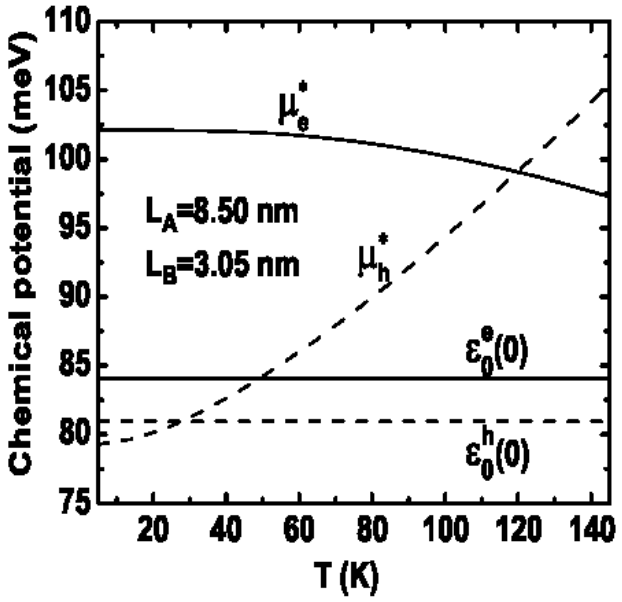

Fig.6 Temperature dependence of the non-equilibrium chemical potentials for electrons (μ_e^*) and holes (μ_h^*) in a type II SL with the fixed InAs/GaSb layer widths L_A/L_B as indicated. The results are shown for $n_e = n_h = 2\times10^{17} cm^{-3}$ per SL cell.

From the results obtained from mini-band structure calculations, we know that in an InAs/GaSb type II SL, the energy spacing among the electron/hole mini-bands in the InAs/GaSb layers (i.e., $\varepsilon_m^j(k_z) - \varepsilon_n^j(k_z) > 100meV$) are much larger than the THz energy. As a result, the THz optical absorption is achieved mainly via type II transition channel, namely through the inter-layer transition between the electron mini-band in the InAs layers and the heavy-hole mini-band in the GaSb layers. The dependence of the optical absorption spectrum on the InAs/GaSb layer widths is shown in Fig. 7 at T = 25 K. Because of a strong type II optical transition in an InAs/GaSb SL, a sharp absorption cut-off can be observed. The rather broad absorption spectrum seen here is induced mainly by the presence of the dispersed electron mini-bands in an SL. We find that a more efficient THz absorption can be observed for samples with larger InAs well widths (compare the upper and lower panels in Fig. 7). For example, a strong absorption (about a factor of 2) at 1 *THz* can be seen for a sample with the well widths 8.50/3.05 *nm* than that with the well widths 6.30/7.90 *nm*. More pronounced cut-off of the THz absorption can be achieved for samples with smaller band-gaps.

In Fig. 8, the dependence of the THz optical absorption on temperature is shown for an InAs/GaSb SL with the fixed well layer thicknesses. As can be seen, the THz optical absorption via type II transition in an InAs/GaSb SL depends strongly on temperature. In particular, the blue-shift of the cut-off absorption can be observed with decreasing temperature at relatively low-temperatures. From Eq. (16) we note that for type II optical transition in a type II SL, there are two kinds of cut-offs for carrier-photon interaction through optical absorption scattering. One is induced by the term $\Theta\left[\varepsilon_0^h(k_z) + \hbar\omega - \varepsilon_0^e(k_z)\right]$, which is required by the momentum and energy conservation laws during a scattering event (Mechanism I). Another is caused by the term

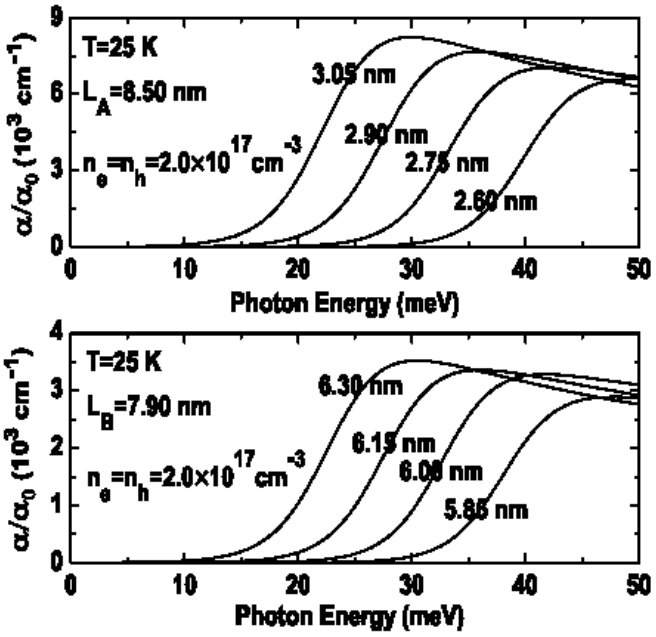

Fig.7 Optical absorption spectrum at a fixed InAs (GaSb) layer width L_A (L_B) for different GaSb (InAs) layer widths, in the upper (lower) panel. The results are shown for $n_e = n_h = 2\times10^{17} cm^{-3}$ per SL cell.

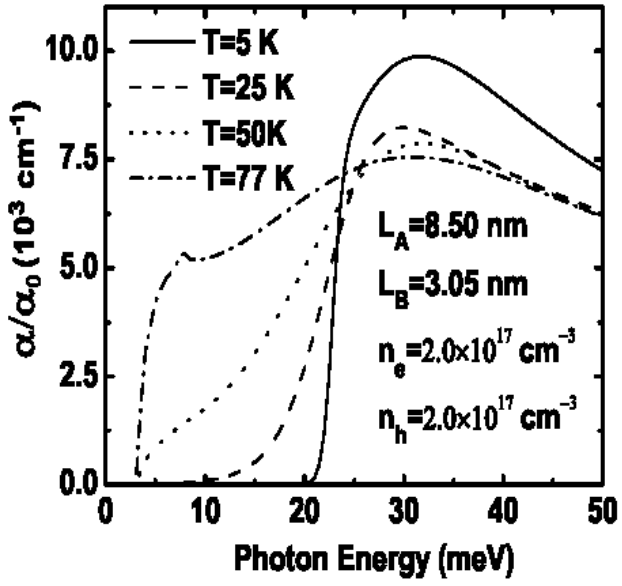

Fig. 8 Temperature dependence of the THz absorption in an InAs/GaSb SL at the fixed InAs/GaSb layer widths L_A/L_B and the fixed carrier densities $n_e = n_h$ per SL cell as indicated.

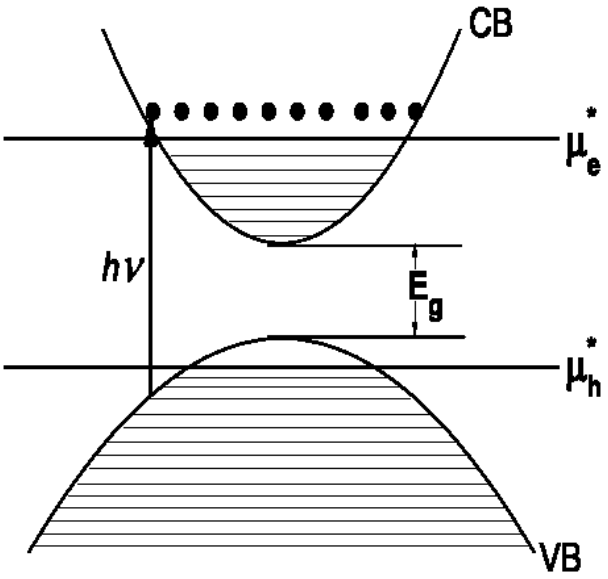

Fig.9 Type II optical transition channel in the presence of photo-excited carries in a type II SL. Here, E_g is the energy-gap between the bottom of electron mini-band in the InAs layer and the top of hole mini-band in the GaSb layer, μ_e^* and μ_h^* are non-equilibrium chemical potentials for the photo-excited electrons and holes respectively.

$f_h(x_e^-)\left[1-f_e(x_j^e)\right]$, which reflects a fact that optical transition can be achieved via exciting electrons in the occupied states in the hole mini-bands in the GaSb layer to the empty states in the electron mini-band in the InAs layer (Mechanism II). We find that for typical InAs/GaSb type II SLs, the Mechanism I results in a cut-off in optical absorption at relatively high temperatures (i.e., T = 77 K in Fig. 8), whereas the Mechanism II is responsible for the absorption cut-off at low-temperatures (i.e., T = 5 K and 25 K in Fig. 8). As can be seen in Fig. 9, for a undoped sample in the presence of photoexcited carriers, there are empty states in the hole mini-band in the GaSb layer owing to the excitation of electrons in the hole mini-band into the electron mini-band. This implies that at low-temperatures, a photon energy $\hbar\omega \geq \Delta = \left(\varepsilon_0^h(0)-\mu_h^*\right)+\left(\mu_e^*-\varepsilon_0^e(0)\right)=E_g+\mu_e^*-\mu_h^*$ is required in achieving optical transition to satisfy the energy conservation law. Because $\mu_e^*(\mu_h^*)$ decreases (increases) with increasing temperature (see Fig. 6), Δ decreases with increasing temperature. Thus, a red-shift of the cut-off absorption can be observed with increasing temperature at relatively low-temperatures. At relatively high-temperatures, the effect of the presence of the non-equilibrium chemical potentials becomes weak due to the thermal broadening of the distribution functions for electrons and holes. As a result, the optical absorption cut-off is mainly achieved via the Mechanism I at relatively high-temperatures. From Fig. 8, it is interesting to note that for an InAs/GaSb type II SL, a sharper cut-off in THz optical absorption can be observed at relatively high-temperatures. This suggests that InAs/GaSb type II SLs can be applied as THz photodetectors working at relatively high-temperatures.

5. Conclusions

In this study, we have found that the fundamental THz band-gap can be realized in InAs/GaSb based type II SLs. Two sets of the growth parameters with the InAs/GaSb layer widths about 8.5/2.8 nm and 6.1/7.9 nm can be used to achieve the THz energy-gap between the bottom of the lowest electron mini-band in the InAs layer and the top of the highest heavy-hole mini-band in the GaSb layer. The THz band-gap decreases with increasing InAs/GaSb layer widths. In such SLs, THz optical absorption can be achieved via type II transition (or inter-layer transition channels) and the cut-off of the absorption spectrum can be observed at THz frequencies. The cut-off frequency is red-shifted with increasing the InAs/GaSb layer widths and/or temperature. We have also found that the sharper cut-off of the THz absorption in such SLs can be observed at relatively high-temperatures. These features favor greatly the application of InAs/GaSb based type II SLs as practical THz photodetectors working at relatively high-temperatures. We hope these theoretical predictions and findings can be verified experimentally.

Acknowledgement

This work was supported by the Chinese Academy of Sciences and the National Natural Science Foundation of China.

References

[1] B. Ferguson and X.C. Zhang, *Nature Materials* 1, 26, (2002).

[2] For a review, see, e.g., P.H. Siegel, IEEE Trans. on Microwave Theory and Tech. 50, 910, (2002).

[3] See, e.g., G. Bastard, *Wave Mechanics Applied to Semiconductor Heterostructures*, Monographies de Physique, Paris, (1992).

[4] H.J. Haugan, F. Szmulowicz, G.J. Brown, and K. Mahalingam, J. *Appl. Phys.* 96, 2580, (2004).

[5] See, e.g., G. Grosso and G.P. Parravicini, *Solid State Physics,* Academic Press, (2000).

[6] W. Xu, F.M. Peeters, and J.T. Devreese, *Phys. Rev.* B 46, 7571, (1992).

[7] W. Xu, Appl. *Phys. Lett*. 89, 171107, (2006).

[8] X.L. Lei and S.Y. Liu, J. *Phys.: Condens. Matter* 12, 4655, (2000).

[9] P.A. Folkes, G. Gumbs, W. Xu, and M.T. Lara, *Appl. Phys. Lett*. 89, 202113, (2006).

[10] W. Xu, P.A. Folkes, and G. Gumbs, J. *Appl. Phys.* 102, 033703, (2007).